ELSEVIER

Ultrasound in Med. & Biol., Vol. 29, No. 2, pp. 239–253, 2003

0301-5629/03/$–see front matter

doi:10.1016/S0301-5629(02)00710-X

● *Original Contribution*

COMPENSATION OF LOG-COMPRESSED IMAGES FOR 3-D ULTRASOUND

JOÃO M. SANCHES* and JORGE S. MARQUES
Instituto Superior Técnico/Instituto de Sistemas e Robótica, Lisbon, Portugal

(*Received* 20 *May* 2002; *in final form* 3 *October* 2002)

Abstract—In this study, a Bayesian approach was used for 3-D reconstruction in the presence of multiplicative noise and nonlinear compression of the ultrasound (US) data. Ultrasound images are often considered as being corrupted by multiplicative noise (speckle). Several statistical models have been developed to represent the US data. However, commercial US equipment performs a nonlinear image compression that reduces the dynamic range of the US signal for visualization purposes. This operation changes the distribution of the image pixels, preventing a straightforward application of the models. In this paper, the nonlinear compression is explicitly modeled and considered in the reconstruction process, where the speckle noise present in the radio frequency (RF) US data is modeled with a Rayleigh distribution. The results obtained by considering the compression of the US data are then compared with those obtained assuming no compression. It is shown that the estimation performed using the nonlinear log-compression model leads to better results than those obtained with the Rayleigh reconstruction method. The proposed algorithm is tested with synthetic and real data and the results are discussed. The results have shown an improvement in the reconstruction results when the compression operation is included in the image formation model, leading to sharper images with enhanced anatomical details. (E-mail: jmrs@alfa.ist.utl.pt)

Key Words: **Image compression, 3-D ultrasound, Multiplicative noise, Speckle.**

INTRODUCTION

Most reconstruction algorithms that have been used in 3-D ultrasound (Nelson et al. 1999; Quistgaard 1997) are simple and fast. They aim to minimize the reconstruction time (Rohling et al. 1999a). Bayesian approaches (Herman and Kuba 1999; Katsaggelos 1991) have been avoided because they are computationally demanding in terms of CPU time and memory requirements. However, the recent evolution of digital computers opens new opportunities for the use of sophisticated estimation methods.

In this paper, the reconstruction of a 3-D data volume from noisy and compressed ultrasound (US) images is addressed. A freehand US probe is used to obtain a sequence of US images, corresponding to cross-sections of the organ to be inspected (see Fig. 1). A spatial locator is used to measure the position of the US probe. Each image is then preprocessed by the US equipment and is usually the only output of the US equipment. The radio-frequency (RF) image is not provided by the equipment and, therefore, is not available for processing. The main goal of 3-D US is the reconstruction of the original volume from this set of compressed US images.

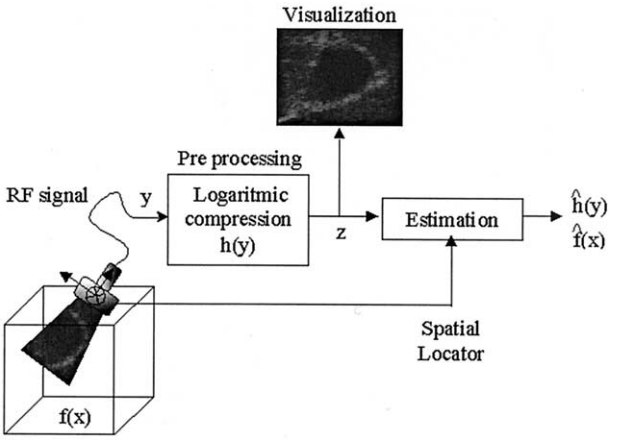

Fig. 1. Block diagram of the processing system.

Several statistical models have been proposed in the literature to model the multiplicative noise (speckle)

Address correspondence to: Dr Joa. M Sanches, Instituto Superior Tecnico, Torn Norte, Sala 6.09, Av Rovisco Pais, 1049-001 Lisbon, Portugal. E-mail: jmrs@alfa.ist.utl.pt

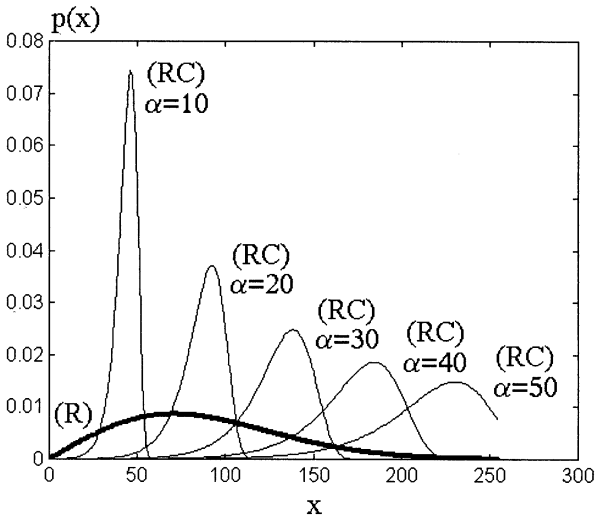

Fig. 2. Distribution functions for the Rayleigh model (*R*) and Rayleigh compressed model (*RC*) with $\alpha = \{10, 20, 30, 40, 50\}$.

present in the RF signal provided by the US probe (Narayanan et al. 1994; Keyes and Tucker 1999). These models were developed for specific organs and tissues, according to their physical and acoustic properties. The Rayleigh distribution (Burckhardt 1978; Abbot and Thurstone 1979; Wells and Halliwell 1981), used in this paper, is a common and simple model used to characterize the speckle noise affecting the US images of soft tissues such as liver and kidney (Achim et al. 2001).

However, the signal is usually filtered and compressed during the preprocessing stage. Compression is used to reduce the dynamic range of the US signal for visualization purposes. Unfortunately, it also modifies the probability distribution, as shown in Fig. 2. A detailed knowledge of the preprocessing operation is usually unavailable, and depends on a set of parameters defined during the medical examination. These parameters are, for example, the brightness, contrast and zoom, defined by the medical doctor during the examination to improve the visualization of a given area or organ. Therefore, the Rayleigh distribution suggested by physics becomes inappropriate, hampering the performance of the reconstruction procedure. To avoid this difficulty, the RF signal (*i.e.*, the signal before preprocessing) is sometimes used in some works (Shankar 1986; Hokland 1996; Cramblitt and Parker 1999). However, when the RF signal is not available, alternative compensation methods are needed. The effect of nonlinear preprocessing has been considered in the past, in the scope of noise reduction with median and adaptative filtering (Loupas et al. 1989; Karaman et al. 1995; Dutt 1996) and will be addressed here in the context of 3-D reconstruction.

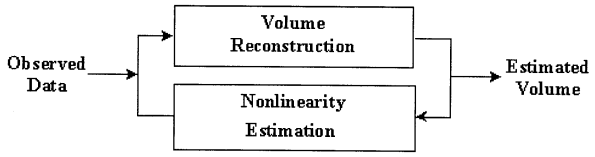

Fig. 3. Block diagram of the reconstruction process.

In this paper, the maximum *a posteriori* (MAP) criterion (Duda and Hart 1973) is used to estimate a 3-D function describing the acoustic properties of a given region from a set of cross-sections. Because the nonlinear operation performed during the preprocessing stage is unknown, it has to be estimated during the reconstruction phase. Because realistic models are required to make the Bayesian algorithm works properly, the preprocessing function should be included in the image formation model.

A two-step approach is proposed, in which reconstruction and nonlinearity identification alternate (see Fig. 3). It is important to note that the improvement in the visualization obtained in the US equipment by the log-compression operation is not useful in the context of Bayesian estimation. In fact, our main concern was to consider the correct model for the observed data to improve the performance of the reconstruction algorithm.

This paper extends the work presented by Sanches and Marques (2000, 2001a, 2001b).

PROBLEM FORMULATION

Consider the experimental setup described in Fig. 1. Given a set of US images and the output of the spatial locator, we wish to estimate a function related to the acoustic impedance in a given volume-of-interest (VOI). Because the preprocessing operation performed by the US equipment is unknown, we also wish to identify this operation to improve the reconstruction results.

Let U be a set of unknown parameters defining the acoustic properties of the volume and let α, β be the parameters defining the preprocessing operation (see details below). Using the MAP estimation method, these parameters are obtained by:

$$(\hat{U},\hat{\alpha},\hat{\beta}) = arg \max_{U,\alpha,\beta} \ln(p(Y|U, \alpha, \beta)p(U)p(\alpha, \beta)), \quad (1)$$

where Y denotes the available data (US images + spatial locator information), $p(Y|U)$ is the sensor model and $p(U)$, $p(\alpha, \beta)$ are the priors associated with the volume coefficients (Ripley 1996) and the nonlinear compres-

sion, respectively.

Because it is not possible to optimize the objective function with respect to all parameters, eqn (1) will be decomposed into two steps:

$$\hat{U} = arg \max_{U} \ln(p(Y|U, (\alpha, \beta))p(U)p(\alpha, \beta)) \quad (2)$$

$$(\hat{\alpha}, \hat{\beta}) = arg \max_{\alpha,\beta} \ln(p(Y|U, (\alpha, \beta))p(U)p(\alpha, \beta)), \quad (3)$$

that correspond to 1. volume reconstruction and 2. preprocessing identification (see Fig. 3). In step 1, the α, β estimates are used to improve the volume reconstruction results and, in step 2, the reconstruction estimate $\hat{U}$ is used for the identification of the image compression parameters α, β. Both steps alternate until convergence is achieved.

The volume description, the data model and the prior distribution used in this paper are described in the next three sections.

Volume description

It will be assumed that the function f describing the volume belongs to a class of admissible functions defined in a spatial domain, $\Omega \subset R^3$ (*i.e.*, $f : \Omega \rightarrow R$). Furthermore, it is assumed that the set of admissible functions is a finite dimension vector space F with known basis functions, $b_i : \Omega \rightarrow R$. Each function $f \in F$ can be expressed as a linear combination of the basis functions, as follows:

$$f(x) = B(x)^T U \quad (4)$$

where $B(x) = [b_1(x), b_2(x), \ldots, b_N(x)]$ is a $N \times 1$ vector of basis functions and $U = [u_1, u_2, \ldots, u_N]$ is a $N \times 1$ vector of coefficients.

It is assumed that each $b_i(x)$ is obtained by shifting a local function $h : R \rightarrow R$:

$$b_i(x) = h(x - \mu_i), \quad (5)$$

where $\mu_i \in R^3$ is the ith node of a cubic grid (see Fig. 4) defined in Ω. Furthermore, h is a trilinear interpolation function defined by:

$$h(x) = \begin{cases} \Pi_{i=1}^{3} \left(1 - \dfrac{|x^i|}{\Delta}\right) & x \in \delta \\ 0 & \text{otherwise} \end{cases}, \quad (6)$$

where x^i is the ith coordinate of x, Δ is the grid step and

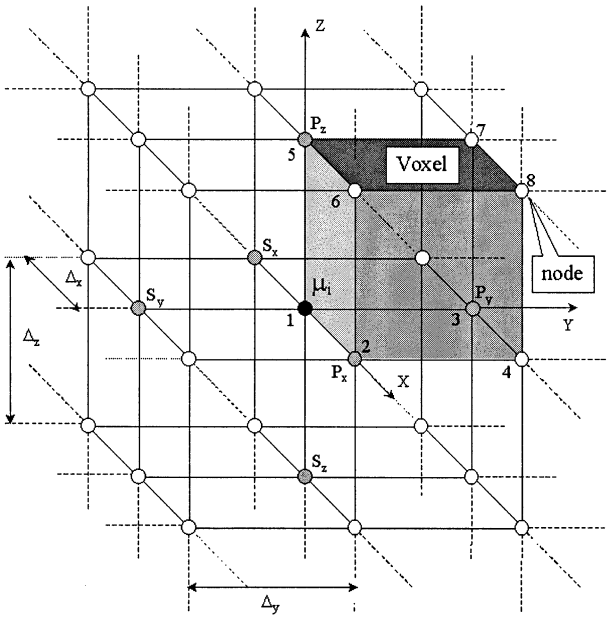

Fig. 4. 3-D cubic grid.

$\delta = [-\Delta, \Delta]^3$.

The grid defines a partition of Ω into cubic voxels. It is concluded from eqns (5 and 6) that each basis function b_i has a finite support of eight voxels and, therefore, each 3-D point belongs to eight support regions. To compute $f(x_0)$, defined in eqn (4), only eight coefficients are needed because all the other basis functions are zero at $x = x_0$.

Data model

The data used to estimate f consist of a sequence of US images complemented with trajectory (position and orientation) of the US sensor during the medical examination. This information allows us to compute a set of data points, $V = \{v_i\}$, containing geometric and intensity information (*i.e.*, $v_i = (z_i, x_i)$ where z_i is the intensity of the pixel located at the position $x_i \in R^3$.

The signal Y generated by the ultrasound probe is a $N \times M$ matrix. It is assumed that Y is a set of i.i.d. (independent and identically distributed) random variables with Rayleigh distribution (Burckhardt 1978; Abbot and Thurstone 1979),

$$p(y_i) = \frac{y_i}{f(x_i)} e^{-\frac{y_i^2}{2f(x_i)}}, \quad (7)$$

where y_i denotes the amplitude of ith pixel of the noncompressed image and $f(x_i)$ is the value of the function f computed at position x_i.

Let Z be the output of the preprocessing block (see

Fig. 1). Statistical independence of all elements of Z is assumed (Dias and Leitao 1996). This assumption is not usually realistic because the PSF (point spread function) of the image-acquisition system is, in general, larger than the interpixel distance. However, it is not easy to estimate the PSF of the acquisition system. This function depends not only on the impulsive response of the US probe and the associated electronics but, also, on the image processing performed by US equipment. In particular, the filtering procedure that smoothes the original raw data by converting the polar structure of the RF signal in the rectangular structure of the observed US images introduces correlation among the pixels that is difficult to model. Furthermore, the improvement achieved in the reconstruction results by considering the statistical dependence among the pixels of the image is not relevant when compared with the computational complexity introduced in the algorithm, as noted by Rignot and Chelappa (1992).

In this paper, a log-compression law is considered:

$$z_i = h(y_i) = \alpha \log(y_i + 1) + \beta, \tag{8}$$

where (α, β) are unknown coefficients. Therefore, the distribution of z is given by:

$$p(z_i) = \left|\frac{dy}{dz}\right| p(y_i), \tag{9}$$

where $p(y)$ is the density function of the noncompressed US image and dy/dz is the derivative of the inverse compression function. Using eqns (7 and 9) leads to the new model for the image formation process:

$$p(z_i/U) = \frac{w_i(w_i + 1)}{\alpha f(x_i)} e^{-\frac{w_i^2}{2f(x_i)}}, \tag{10}$$

where

$$w_i = e^{\frac{z_i - \beta}{\alpha}} - 1, \tag{11}$$

and (α, β) are the unknown parameters of the compression law to be estimated. The reconstructions using this new model (RC, Rayleigh compressed) are compared with the Rayleigh model (R) in the section on Experimental Results.

The log likelihood function for this problem is thus defined by:

$$l(U, \alpha, \beta) = \sum_i \left[\log\left(\frac{w_i(w_i + 1)}{f(x_i)\alpha}\right) - \frac{w_i^2}{2f(x_i)} \right]. \tag{12}$$

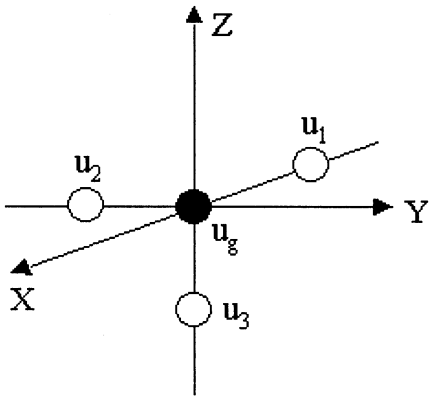

Fig. 5. Neighbor system.

Prior model

Three dimensional US involves the interpolation of measured data between the inspection planes, as well as the ability to perform data fusion and noise reduction. Some assumptions must be made to interpolate the data. This information is included in the prior distribution. In this work, a Gibbs prior is used, based on a set of quadratic potential functions (Geman and Geman 1984). These functions are used to guarantee the smoothness of the spatial coefficients. They introduce a regularization effect that allows us to recover the unknown coefficients, even when no data are observed in a given region. In addition, regularization also improves the convergence of the optimization algorithm. The choice of a Gibbs distribution is equivalent to considering U as a Markov random field, as stated by the Hammersley–Clifford theorem (Marques 1999). The prior distribution adopted in this paper is:

$$p(U) = Ce^{-\Psi \sum_{g\in\Gamma} \sum_{j=1}^{3} (u_g - u_{gj})^2}, \text{ by } p(U) = Ce^{-\Psi \sum_{g\in\Gamma}\sum_{j=1}^{3}(u_g - u_{gj})^2} \tag{13}$$

where Γ is the set of all grid indices of the 3-D cubic grid, u_{gj} is the jth neighbor of u_g, as shown in Fig. 5, and C is a normalization factor.

The ψ parameter measures the strength of the connections among neighboring nodes. High values of ψ correspond to strongly connected neighbors (differences receive a high penalty) and low values of ψ correspond to weak connections. It is often convenient to assume that ψ varies during the optimization process, starting with a high value that is gradually reduced (Figueiredo and Leitao 1993). In this paper, the parameter ψ is defined manually. The best choice is obtained by trial and error (*i.e.*, by testing a set of values and selecting the one that leads to better results).

PARAMETER ESTIMATION

The estimation of the U coefficients is performed by the MAP method, leading to the maximization of the joint density function $p(Z, U, \alpha, \beta)$. This is a difficult problem because the number of parameters to estimate is very large (typically, thousands of coefficients) and $p(Z, U, \alpha, \beta)$ is a nonconvex function (Li 1998). Simpler expressions are obtained by using $g(U, \alpha, \beta) = \log p(Z, U, \alpha, \beta)$, leading to:[1]

$$g(U, \alpha, \beta) = \sum_i \left[\log\left(\frac{w_i (w_i + 1)}{f(x_i)\alpha} \right) - \frac{w_i^2}{2f(x_i)} \right] - \psi \sum_{g \in \Gamma} \sum_{j=1}^{3} (u_g - u_{gj})^2. \quad (14)$$

However, the key difficulties that were described above remain the same. One way to maximize g is by finding a stationary point of eqn (14) with respect to each unknown variable. This topic will be addressed in the next sections.

Volume reconstruction

In this paper, each component u_p of U is sequentially updated by the ICM (iterated conditional modes) algorithm proposed by Besag (1986). In this algorithm, for each iteration, all the unknown variables are sequentially estimated considering eqn (14) as an unidimensional function of u_p. A unidimensional version of the Newton–Raphson method (Press et al. 1994) is used to solve:

$$\frac{\partial}{\partial(u_p)} g(u_p) = 0, \quad (15)$$

leading to

$${}^{n+1}\hat{u}_p = {}^{n}\hat{u}_p + \lambda \frac{0.5 \sum_i \frac{w_i^2 - 2f(x_i)}{f^2(x_i)} b_p(x_i) - 2\psi N_v (u_p - \bar{u}_p)}{\sum_i \frac{w_i^2 - f(x_i)}{f^3(x_i)} b_p^2(x_i) + 2\psi N_v} \quad (16)$$

with

$$\bar{u}_p = \frac{1}{N_v} \sum_{u_g \in \delta_p} u_g, \quad (17)$$

where ${}^{n}\bar{u}_p$ is the estimate of u_p obtained at the nth iteration, N_v is the number of control points inside the neighborhood δ_p of the pth grid node $p(N_v = 6)$ and λ is a gain.

To implement the reconstruction algorithm using the Rayleigh model, eqn (16) can be used by making $w_i = z_i$.

Nonlinearity estimation

To estimate (α, β), a bidimensional version of the Newton–Raphson algorithm is used, that is:

$$({}^{n+1}\hat{\alpha}, {}^{n+1}\hat{\beta}) = ({}^{n}\hat{\alpha}, {}^{n}\hat{\beta}) - \nabla g(\hat{U}, {}^{n}\hat{\alpha}, {}^{n}\hat{\beta}) H^{-1} \quad (18)$$

where $\nabla g\ (U, \alpha_0, \beta_0)$ is the gradient vector and H is the Hessian matrix with respect to α, β. Equation (18) can be rewritten as follows:

$${}^{n+1}\hat{\alpha} = {}^{n}\hat{\alpha}\left(1 - \xi_\alpha \frac{g_\beta g_{\alpha\beta} - g_\alpha g_{\beta\beta}}{g_{\alpha\alpha} g_{\beta\beta} - g_{\alpha\beta}^2} \right) \quad (19)$$

$${}^{n+1}\hat{\beta} = {}^{n}\hat{\beta}\left(1 - \xi_\beta \frac{g_\alpha g_{\alpha\beta} - g_\beta g_{\alpha\alpha}}{g_{\alpha\alpha} g_{\beta\beta} - g_{\alpha\beta}^2}, \right. \quad (20)$$

where

$$g_\alpha = \frac{1}{\alpha} \sum_i [A_i \log(w_i + 1) - 1] \quad (21)$$

$$g_\beta = \frac{1}{\alpha} \sum_i A_i \quad (22)$$

$$g_{\alpha\alpha} = -\frac{1}{\alpha^2} \sum_i [2A_i \log(w_i + 1) + B_i \log^2(w_i + 1) - 1] \quad (23)$$

$$g_{\beta\beta} = -\frac{1}{\alpha^2} \sum_i B_i \quad (24)$$

$$g_{\alpha\beta} = -\frac{1}{\alpha^2} \sum_i [A_i + B_i \log(w_i + 1)] \quad (25)$$

$$A_i = \frac{w_i^3 + w_i^2 - 2f(x_i)w_i - f(x_i)}{f(x_i)w_i} \quad (26)$$

[1]The constant C was discarded because it does not contribute to the solution.

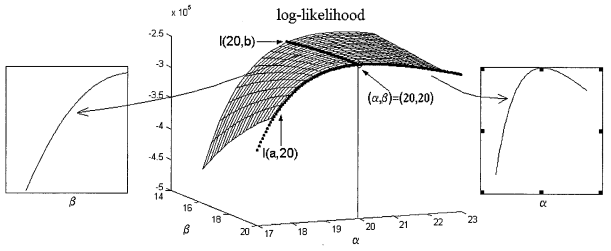

Fig. 6. Likelihood surface and profiles; 65535 pixels, Rayleigh-distributed and log-compressed, with $(\alpha, \beta) = (20, 20)$.

$$B_i = \frac{2w_i^3 + w_i^2 + f(x_i)}{f(x_i)w_i^2}(w_i + 1), \tag{27}$$

and ξ_α, ξ_β are update gains.

It should be stressed that the estimation of (α, β) requires an estimate of the volume coefficients, $\hat{U}$. The converse is also true. Volume reconstruction assumes that (α, β) estimates are available. Improved α and β estimates allow us to achieve improved volume reconstruction and *vice versa.* This suggests a recursive procedure in which both steps alternate.

Figure 6 shows the dependence of the likelihood function on (α, β) parameters. The log-likelihood profiles associated with the global maximum are also shown. The maximum is achieved near the true values of the parameters: $\alpha = \beta = 20$. This image shows a flat surface with a nonpronounced maximum, which leads to difficulties in the estimation of accurate solutions. On the other hand, this means that the reconstructed volumes are not sensitive to the estimated preprocessing parameters (α, β).

One of the synthetic images used in this example is shown in Fig. 7a, which displays the original image, with random Rayleigh-distributed pixels. The histogram of the pixel intensity is shown below.

Figure 7b shows the log-compressed image obtained by applying the nonlinear transformation eqn (8) to the pixels of the original image with parameters $\alpha = \beta = 20$. The histogram is no longer Rayleigh, as shown below. Finally, Fig. 7c shows the estimated image using the log-compressed model. It is concluded that the estimated image is similar to the original image, with both histograms almost identical, as expected, showing the ability of the algorithm to recover the original data.

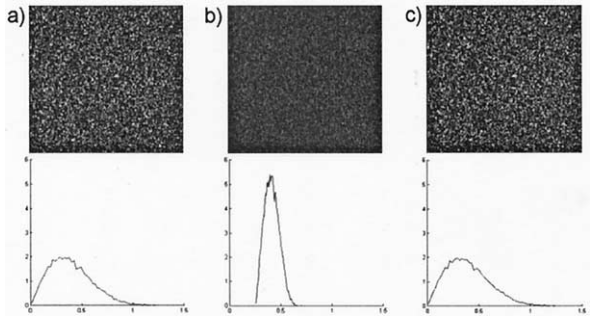

Fig. 7. Restoration results: Images and histograms; (a) original (Rayleigh), (b) Observed (compressed), and (c) decompressed.

During the estimation process, the parameter estimates must be monitored to avoid values with no physical meaning. Two cases should be considered. Volume coefficients should be greater than zero. In addition, the Rayleigh distribution has a singularity for zero values of the parameter *f.* Therefore, the reconstructed volume must be strictly positive. The second problem concerns the offset constant, β_0: β must always be smaller than min(z). Otherwise:

$$w_i = e^{\frac{z_i - \beta}{\alpha}} - 1 \tag{28}$$

would take nonpositive values, which is not possible.

Initialization procedure

Equations (2) and (3) define a recursive algorithm to update the volume and preprocessing estimates. However, the algorithm must be initialized with reasonable estimates of these parameters. In fact, the optimization results and convergence rate depend on this initial guess. In this section, expressions for the initial estimates are derived.

A different compression model will be considered for convenience; compare with eqn (8):

$$z = \alpha \log(y) + \beta. \tag{29}$$

Assuming that y is a random variable with Rayleigh distribution, $p(z)$ becomes a Fisher–Tippet distribution, also known as double exponential distribution (see Appendix A for details) (Abramowitz and Stegan 1972; Dutt 1996).

$$p(z_i/U) = \frac{w_i^2}{\alpha f(x_i)} e^{-\frac{w_i^2}{2f(x_i)}} \tag{30}$$

where

$$w_i = e^{\frac{z_i - \beta}{\alpha}} \tag{31}$$

As can be verified, this distribution is similar to eqn (10) for the range of values used in US images ($0 \leq z_i \leq 255$), making it possible to approximate eqn (10) by eqn

(30). The expressions for the mean and SD of this distribution are (Abramowitz and Stegan 1972):

$$\bar{z} = \alpha(\log(2f(x)) - \gamma)/2 + \beta \tag{32}$$

$$\sigma_z = \pi\alpha/\sqrt{24} \tag{33}$$

where $\gamma = 0.5772\ldots$ is the Euler–Mascheroni constant.

Based on the above expressions, initial values for the α, u parameters can be computed as follows:

$$\hat{\alpha}_0 = \sqrt{\frac{24}{\pi^2}\sigma_z^2} \tag{34}$$

and

$$\hat{u}_p^0 = 0.5e^{\frac{2\pi(\bar{z}-\min z)}{\sqrt{24\sigma_z^2}}+\gamma} \tag{35}$$

The parameter β will be initialized by:

$$\hat{\beta}_0 = min(z). \tag{36}$$

It was experimentally found that this initialization usually provides a good estimate of β. In fact, this is an expected result because $\min(z) = \min(\log(y + 1) + \beta) = \log(\min(y) + 1) + \beta = \log(0 + 1) + \beta = \beta$. However, this estimator of β_0 is biased with a bias depending on the amount of observed data, as shown in Appendix B.

When the estimation is performed using the Rayleigh model without compensation, the only initialization needed is the one associated with the volume coefficients. In this case:

$$u_p^0 = \frac{2\bar{z}^2}{\pi}. \tag{37}$$

This expression was derived from the mean value of a set with Rayleigh distribution:

$$\bar{z} = \sqrt{\frac{f\pi}{2}}, \tag{38}$$

where f is the parameter of the Rayleigh distribution.

To assess the performance of the initialization procedure for α_0 and β_0, a set of Monte Carlo tests was performed using uniform synthetic data. A set of 100 images with 128 × 128 pixels corrupted with Rayleigh noise and compressed with several pairs of parameters (α, β), was used. For each pair of parameters (α, β), 20 initializations (α_0, β_0) were computed and their mean and SD displayed in Fig. 8a and b.

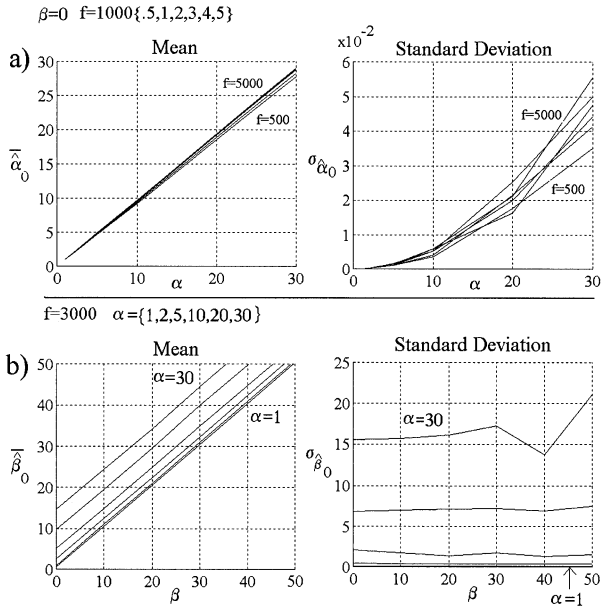

Fig. 8. (a) Mean and SD of the initial α estimates and (b) Mean and SD of the initial β estimates obtained by Monte Carlo tests. Each simulation was performed using a set of 100 images with 128 × 128 pixels.

Figure 8a shows the α statistics for several values of the Rayleigh parameter, f = {500, 1000, 2000, 3000, 4000, 5000}, and the (α, β) pair of parameters. As can be seen, the estimator of α_0 is insensitive to the Rayleigh parameter (magnitude of the data). However, the SD of $\hat{\alpha}_0$ grows with the f parameter. Other experiments made in this context show that α, β estimators are not sensitive to the parameter β. Figure 8b displays the mean and SD for $\hat{\beta}_0$ initial estimates. These results show that there is noticeable dependence of $\hat{\beta}_0$ estimates with respect to α, as is proven in Appendix B. The best results are achieved for low α values.

EXPERIMENTAL RESULTS

This section presents reconstruction results with synthetic and real data. Two methods are considered: 1. the Rayleigh reconstruction algorithm without nonlinearity compensation, eqn (16) with $w_i = z_i$, and 2. the reconstruction algorithm with compensation, eqns (16, 19 and 20). Three problems are considered in this section: 1. the reconstruction of synthetic uniform volumes, 2. the reconstruction of synthetic nonuniform volumes and 3. the reconstruction of medical data. Whenever possible, statistics are provided to assess the performance of both reconstruction algorithms in each of these problems. The reconstruction times depend on the number and dimensions of the images and on the type of processor used. All the experiments presented in this paper

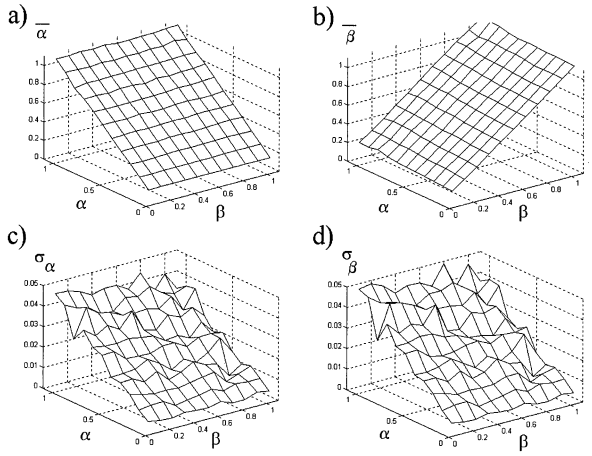

Fig. 9. Mean and SD of ($\hat{\alpha}$ and $\hat{\beta}$) ($\psi = 1$). Results obtained with 20 Monte Carlo runs with uniform images with log-compressed Rayleigh distribution.

were performed in a Pentium III running at 1 GHz. With this processor, for instance, each iteration of the reconstruction algorithm using the thyroid and eyeball sequences (100 images with 128 × 128) takes approximately 30 s to be completed. However, it is possible to adopt several measures to speed up the reconstruction time, as shown by Sanches and Marques (2001a, 2001b, 2002a, 2002b).

Uniform volumes

An example earlier was shown with uniform synthetic data (Fig. 7), where it is clear that the proposed algorithm manages to restore the original distribution of the data, and estimate parameters of the nonlinear compression law. Here, a more complete set of tests is presented to characterize the performance of the algorithm.

Figure 9 shows the mean and SD of $\hat{\alpha}$, $\hat{\beta}$ as a function of the true parameters. These results were obtained with 20 Monte Carlo runs. In each run, the parameters were estimated using a set of 50 uniform cross-sections with 128 × 128 pixels. It was experimentally observed that the MAP estimates are unbiased and that their SD increases linearly with the parameter α.

Nonuniform volumes

Let us now consider the reconstruction of nonuniform volumes. For the sake of simplicity, it is assumed that the function $f(x)$ to be estimated is binary: it has a high value inside the object to be reconstructed and a low value outside. A cube was used in these experiments (see Fig. 10a).

Several experiments were performed. In each experiment, 50 cross-sections of the object are computed.

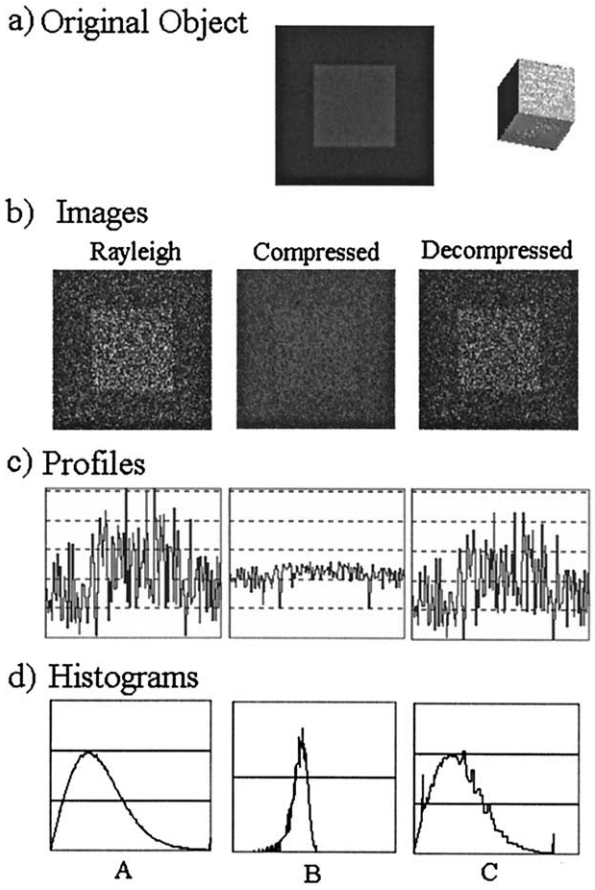

Fig. 10. Reconstruction/restoration results using a 3-D synthetic cube. Data: set of 50 cross-sections corrupted by Rayleigh noise and log-compressed with $\alpha = 20$, $\beta = 20$. (a) Original object, (b) original Rayleigh cross-section, compressed image used in the reconstruction, image decompressed with the inverse of the estimated preprocessing function ($\hat{\alpha} = 20.5$, $\hat{\beta} = 19.7$). (c) Profiles, (d) histograms.

The Rayleigh-distributed images, Fig. 10b,A, are compressed by the log-compression law using selected values for (α, β) parameters, Fig. 10b,B, and used as observations to perform the volume reconstruction and estimation of the preprocessing function. Then, the algorithm described in this paper is used simultaneously to reconstruct the volume and to estimate the (α, β) parameters. Figure 10b,C, shows an example of decompressed image using the inverse of the estimated preprocessing function. As is shown, the original (Fig. 10b,A) and the decompressed (Fig. 10b,C) are very similar. The comparison of the profiles (Fig 10c,A,C) and the histograms of the sequences (Fig. 10d,A,C) confirm this similarity.

Table 1 shows the performance of both models for three different values of $\alpha = \{1, 10, 50\}$ and for $\beta = 0$. The likelihood function and the SNR are the figures of merit used for comparison. This table shows a clear

Table 1. Simulation results with synthetic data (cube)

Compensation									No compensation		
α			β								
α	α_0	$\hat{\alpha}$	β	β_0	$\hat{\beta}$	U_0	$l^* \times 10^6$	SNR (dB)	U_0	$l^* \times 10^6$	SNR (dB)
1.0	0.99	1.00	0.0	0.0	0.0	2835	−10.8	6.3	10.33	−27.5	−38.0
10.0	9.99	10.04	0.0	0.0	0.0	2835	−40.7	6.3	1032.85	−53.0	3.4
50.0	49.94	50.20	0.0	0.0	0.0	2835	−61.5	6.3	25821.36	−80.4	1.5

*log-likelihood.

improvement in the log-likelihood values, as well in the SNR for the reconstruction results using the nonlinear compensation. The estimates of (α, β) parameters obtained in these experiments are close to the original ones. In fact, excellent results are provided by the Fisher–Tippet initialization procedure. Figure 11 show profiles extracted from the estimated volumes for each configuration of the compression law using both models. Fig. 11a, b, c shows the results obtained without compensation and Fig. 11d shows the estimated profiles using compensation.

The reconstruction results obtained with nonlinearity estimation, proposed in this paper, are clearly better than the ones obtained by a straightforward application of the Rayleigh reconstruction algorithm. It should be stressed that the estimated volumes obtained with image compensation are almost invariant with respect to the values of (α, β) parameters (Fig. 11d). It is important to note that the estimations with the Rayleigh models strongly depend on the α parameter (see the vertical scales on Fig. 11a, b, c). On the contrary, using the Rayleigh compressed model, all the reconstructions approximate the original object.

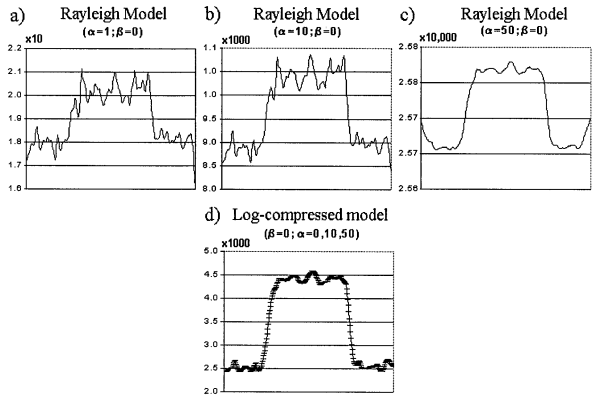

Fig. 11. Profiles extracted from estimated volumes using the: (a) Rayleigh model with $\alpha = 1$ and $\beta = 0$; (b) Rayleigh model with $\alpha = 10$ and $\beta = 0$; (c) Rayleigh model with $\alpha = 50$ and $\beta = 0$; (d) Rayleigh compressed model for $\alpha = 0$, 10, 50 and $\beta = 0$. In this last graph, the vertical bars represent the SD of the estimation for the several values of the compression parameters.

Medical data

The proposed algorithm was used for the reconstruction of human organs using sequences of US images. Three examples are considered, corresponding to the reconstructions of a thyroid, an eye/ball and a gall/bladder. In the first two cases, 100 images with 128 × 128 pixels were available. In the third case, 62 images with 176 × 176 pixels were used.

Figures 12–17 show the reconstruction results (images and profiles) obtained without and with compensation. Figures 12a, 14a, and 16a show four data images of the organ considered (thyroid, eyeball and gall bladder) and intensity profiles along specific lines (see Figs 12b, 14b, 16b).

Figures 13a, d, 15a, d, 17a, d show the corresponding images obtained from the estimated volumes using the Rayleigh and Rayleigh compressed models, respectively. Figures 13b, c, 15b, c, and 17b, c show the profiles extracted from the images displayed in (a) and (d), respectively.

The decompressed images generated by filtering the input images with the inverse of the estimated nonlinearity function are also shown in Figs. 12c, 14c, and 16c.

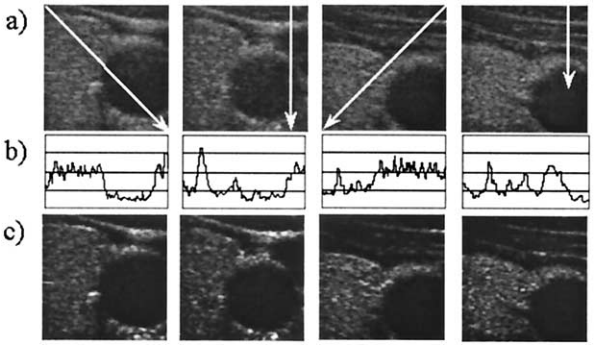

Fig. 12. Thyroid: (a) original images; (b) Original profiles; and (e) Decompressed images.

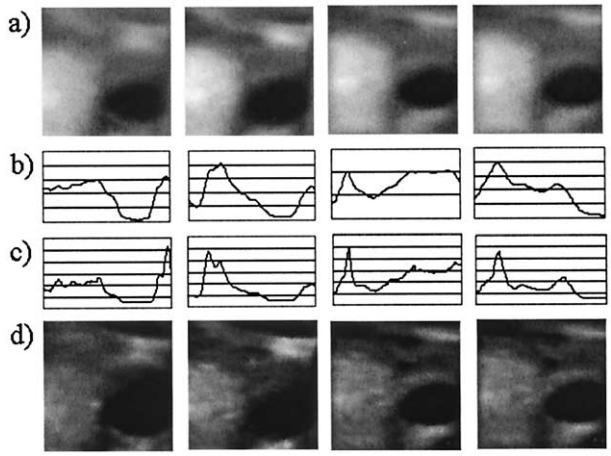

Fig. 13. Thyroid: (a)–(b) Images and profiles extracted from the reconstructed volume using the Rayleigh model (*R*); (c)–(d) images and profiles extracted from the reconstructed volume using the Rayleigh compressed model (*RC*).

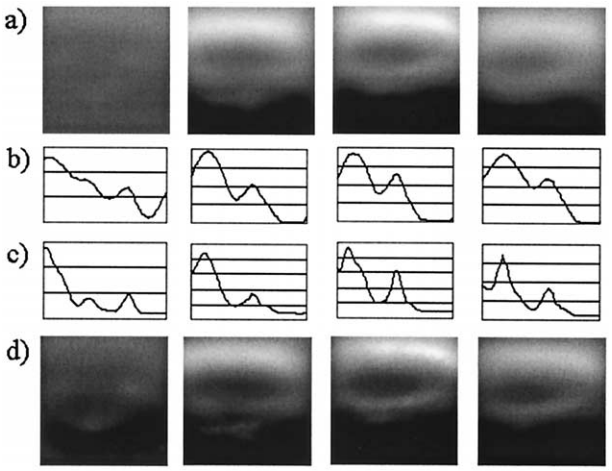

Fig. 15. Eyeball: (a)–(b) images and profiles extracted from the reconstructed volume using the Rayleigh model (*R*); (c)–(d) images and profiles extracted from the reconstructed volume using the Rayleigh compressed model (*RC*).

The decompression functions estimated during this experiment are represented in Fig. 18 for the three organs considered. We have used these functions to generate a new sequence from the observed ones. Some of these new images are represented in Figs. 12c, 14c, and 16c. These images are our estimates of the unobserved RF signal. The histograms of the compressed (A) and decompressed (B) images are shown in Fig. 19. To allow a visual comparison of the two sequences, the decompressed images were scaled to make equal the variance of both sequences.

It is concluded that the algorithm presented in this paper provides a better representation of details with sharper and well-defined transitions, as shown in Figs. 13, 15, and 17. Figure 13a–b, Fig. 15a–b and Fig. 17a–b show cross-sections and profiles extracted from the reconstructed volumes using the Rayleigh model (without nonlinearity compensation) and Fig. 13c–d, Fig. 15c–d and Fig. 17c–d show the reconstruction results using the compensated model.

Table 2 summarizes the estimation results using medical data. In this table, it is possible to observe that the likelihood values computed with image compensation are bigger than the one obtained without compensation. Figure 20 shows the evolution of these values along the reconstruction process for the three organs considered. The use of image compensation allows a significant improvement of convergence rate.

These results, images, profiles and figures of merit suggest that the model that includes the compression preprocessing procedure describes better the observed data and, therefore, is more realistic. With important practical consequences, is the fact that the anatomical details, in the estimated volumes using image compensation, are sharper and well defined, which is relevant in a clinical point of view.

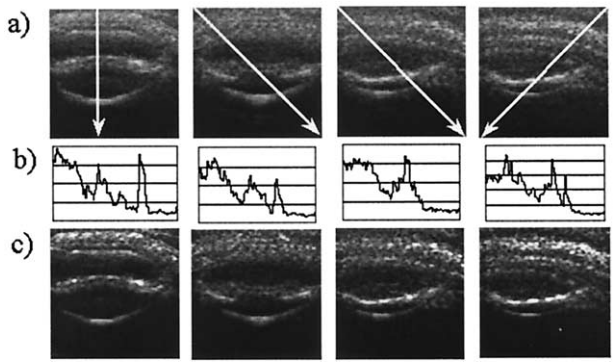

Fig. 14. Eyeball: (a) original images: (b) Original profiles; and (e) Decompressed images.

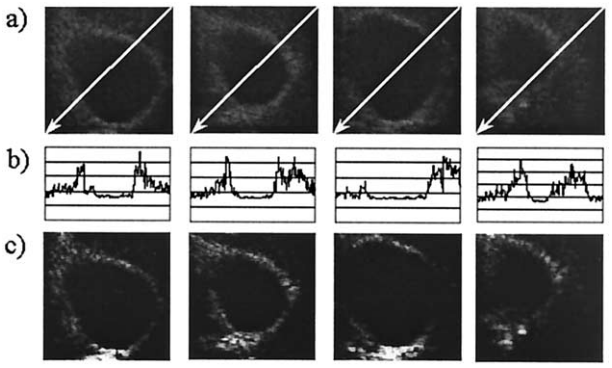

Fig. 16. Gall bladder: (a) original images; (b) Original profiles; and (e) decompressed images.

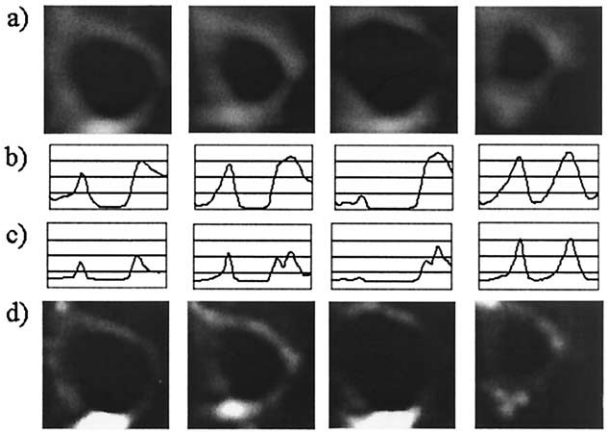

Fig. 17. Gall bladder: (a)–(b) images and profiles extracted from the reconstructed volume using the Rayleigh model (*R*); (c)–(d) images and profiles extracted from the reconstructed volume using the Rayleigh compressed model (*RC*).

It should be noted that the parameter β does not change from its initial guess. The justification for this, in the case of the synthetic data used, is simple. First, we impose $\beta > 0$ and second, $\beta < \beta_0 = \min\{Z\} = 0$, as noted on the Nonlinearity Estimation section. Therefore, with these data, β cannot increase or decrease from the initial guess.

In the case of the real data, β can decrease, because $\beta_0 > 0$. However, because the distribution of the observed data does not perfectly match the distribution of the model, the algorithm tries to increase β, which is not possible ($\beta < \beta_0$). Despite this invariance on the β estimates, it is important to perform its estimation jointly with α to improve the estimation of this last parameter.

CONCLUSIONS

This paper presents an algorithm to estimate a function, $f(x)$, describing the acoustic properties of a given ROI from a set of us images. A Bayesian approach is used to estimate this function, by assuming that the position and orientation of the us probe are accurately known. The log-compression process performed by the preprocessing stage of the us equipment is explicitly considered and compensated. The estimation of the log-compression parameters is simultaneously performed with the volume reconstruction by optimizing an objective function (posterior density function of the unknown parameters).

The optimization process depends on the initialization of the volume and compensation parameters. An initialization procedure is derived, approximating the observation model by a Fisher–Tippett distribution function that leads to accurate initial estimates for α, β, U.

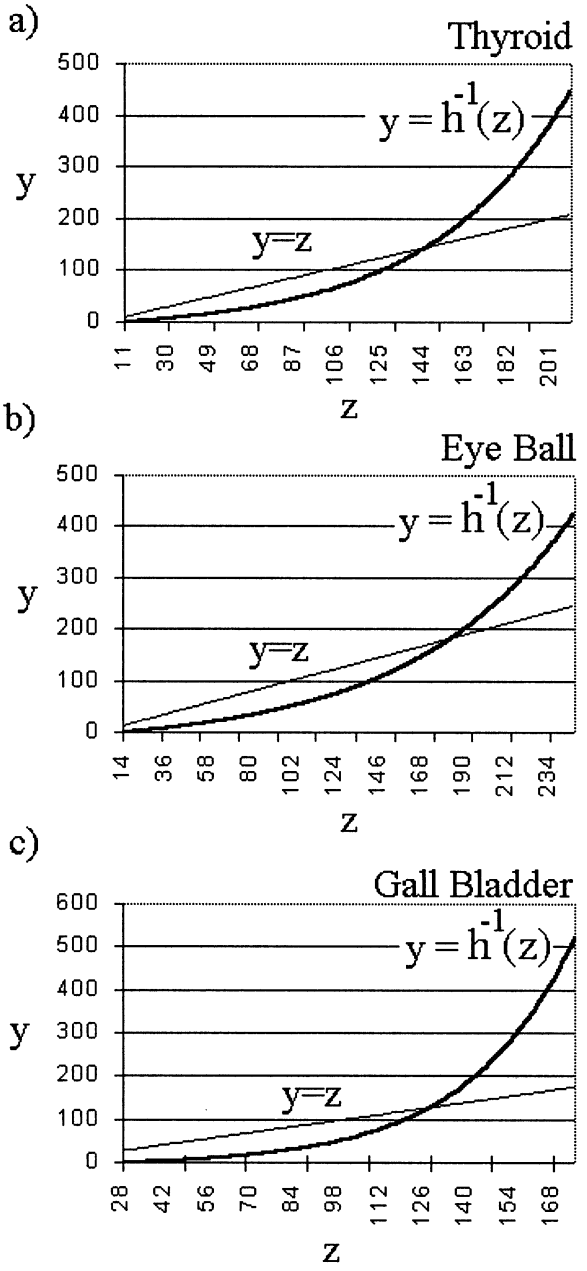

Fig. 18. Estimated decompression functions, $y = h^{-1}(z)$ (thick line) and $y = z$ (thin line). (a) Thyroid, (b) eyeball, (c) gall bladder.

A set of Monte Carlo tests were performed to evaluate the estimates. For each configuration of (α, β), 20 experiments were performed and the mean and SD were computed. It was found that the estimator is unbiased and the SD increases with the α.

Examples of application of the algorithm using synthetic and real data are also presented. In the synthetic case, a set of 50 compressed images, computed from the

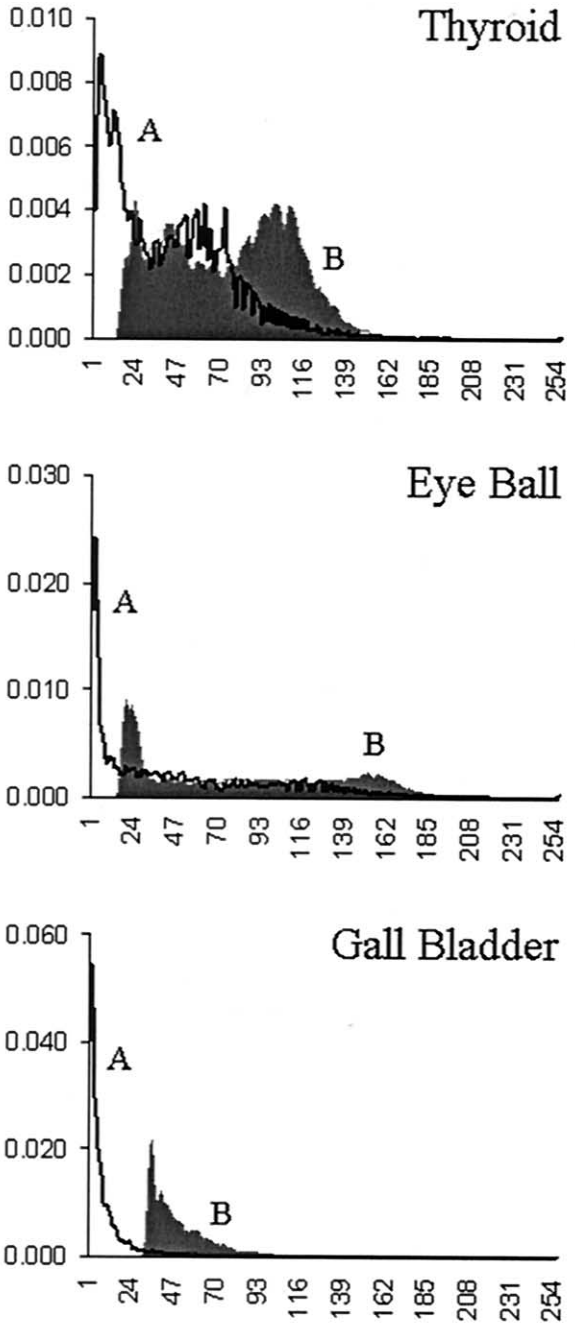

Fig. 19. Histograms of (A) Compressed and (B) Decompressed images. The decompressed images were scaled to make their variance equal to the variance of the original sequence. This procedure is important to allow the visual comparison of the two sequences.

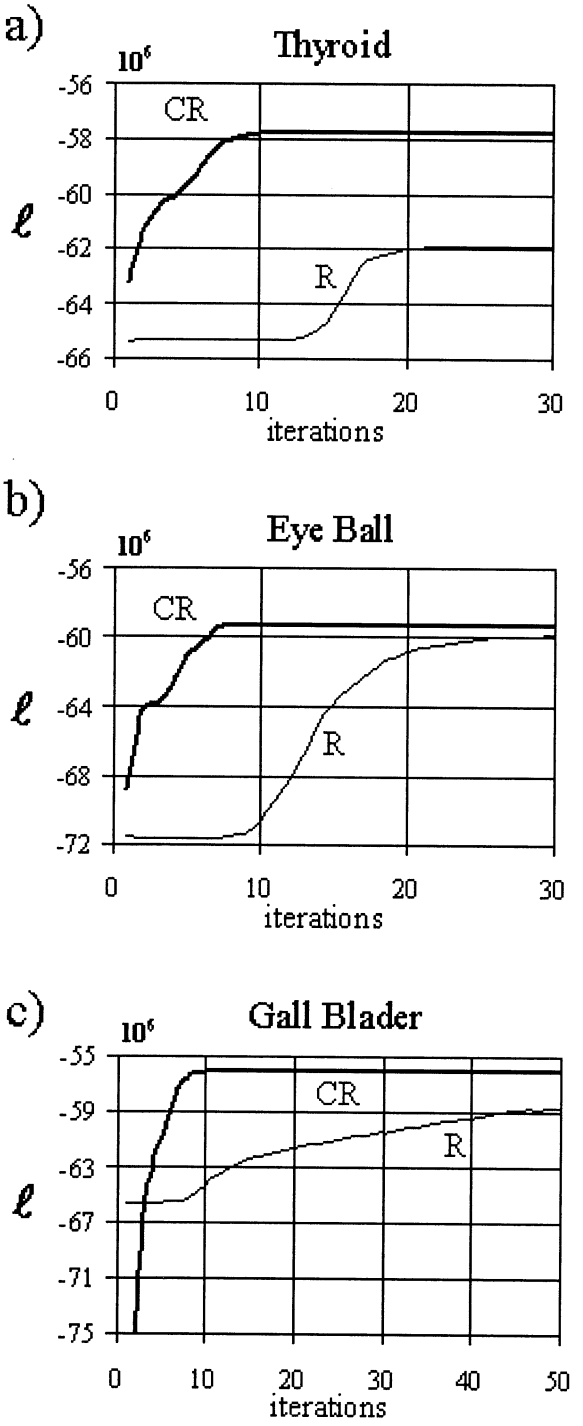

Fig. 20. Evolution of the log-likelihood values with compressed Rayleigh (*CR*) model (thick line) and with Rayleigh (*R*) model (thin line) for the (a) thyroid, (b) eyeball and (c) gall bladder.

cross-sections of a cube and corrupted by Rayleigh noise, is used. The experimental results show that the proposed algorithm manages to retrieve the log-compression parameters and to estimate the original object. Furthermore, it is shown that the results obtained by using image compensation are better than the ones obtained without compensation and not sensitive to the preprocessing parameters.

Table 2. Simulation results with real data

	Compensation						No compensation	
	α		β					
Organ	α_0	$\hat{\alpha}$	β_0	β	U_0	$1^* \times 10^6$	U_0	$1^* \times 10^6$
Thyroid	53.8	61.4	11.0	11.0	9.3	−5.8	3502	−6.2
Eyeball	84.1	82.5	14.0	14.0	4.8	−5.9	4567	−6.0
Gall bladder	28.2	34.8	28.0	28.0	4.2	−5.6	304	−5.9

The proposed algorithm was also applied for the reconstruction of human organs. The experimental results obtained with the proposed algorithm outperform the ones achieved without compensation: the estimated images and profiles obtained by compensating the log-compressed images are sharper, presenting a larger dynamic range, and the anatomical details appear more clear. Furthermore, the figures of merit computed for these sequences, prove that the compressed model fits the observed data better than the Rayleigh model. Finally, and for these real sequences, it was observed an increasing in the convergence rate.

Acknowledgments—This work was partially supported by FCT under project Heart 3-D (Sapiens). The US images were kindly provided by R. Prager and A. Gee from the University of Cambridge.

REFERENCES

Abbot J, Thurstone F. Acoustic speckle: Theory and experimental analysis. Ultrasound Imaging 1979;1:303–324.

Abramowitz M, Stegun IA. Handbook of mathematical functions with formulas, graphs, and mathematical Tables. 9th ed. New York: Dover, 1972.

Achim A, Bezerianos A, Tsakalides P. Novel Bayesian multiscale method for speckle removal in medica ultrasound images. Trans Med Imaging 2001;20(8):772–783.

Besag J. On the statistical analysis of dirty pictures. J R Statist Soc B 1986;48(3):259–302.

Burckhardt C. Speckle in ultrasound B-mode scans. IEEE Trans Sonics Ultrason 1978;SU-25(1):1–6.

Cramblitt RM, Parker KJ. Generation of non-Rayleigh speckle distribution using marked regularity models. IEEE Trans Ultrason Ferroelec Freq Control 1999;46(4):867–874.

Dias J, Leitão J. Wall position and thickness estimation from sequences of echocardiograms images. IEEE Trans Med Imaging 1996;15: 25–38.

Dutt V. Adaptative speckle reduction filter for log-compressed B-scan images. IEEE Trans Med Imaging 1996;15(6):802–813.

Duda RO, Hart PE. Pattern classification and scene analysis. John Wiley & Sons, 1973.

Figueiredo MAT, Leitao JMN. Simulated tearing: An algorithm for discontinuity-preserving visual surface reconstruction. IEEE Computer Society Conference on Computer Vision and Pattern Recognition, New York, NY, June, 1993.

Geman S, Geman D. Stochastic relaxation, Gibbs distributions, and the Bayesian restoration of images. IEEE Trans Pattern Anal Machine Intell 1984;6(6):721–741.

Herman GT, Kuba A. Discrete tomography, foundations, algorithms, and applications. Birkhauser, 1999.

Hokland JH. Markov models of specular and diffuse scattering in restoration of medical ultrasound images. IEEE Trans Ultrasound Ferroelec Freq Control 1996;43(4):660–669.

Karaman M, Kutay MA, Bozdagi G. An adaptative speckle suppression filter for medical ultrasonic imaging. Trans Med Imaging 1995; 14(2):283–292.

Katsaggelos AK. Digital image restoration. Springer Series in Information Sciences. Springer-Verlag, 1991.

Keyes TK, Tucker WT. The K-distribution for modeling the envelope amplitude of a backscattered signal. IEEE Trans Ultrason Ferroelec Freq Control 1999;46(4).

Li SZ. Close-form solution and parameter selection for convex minimization-based edge-preserving smoothing. IEEE Trans Pattern Anal Machine Intell 1998;20(9):916–932.

Loupas T, McDicken WN, Allan PL. An adaptative weighted median filter for speckle supression in medical ultrasonic images. IEEE Trans Circuits Syst 1989;36(1):129–135.

Marques JS. Pattern recognition. Statistical and neuronal approaches. IST Press, 1999.

Narayanan VM, Shankar PM, Reid JM. Non-Rayleigh statistics of ultrasound backscattered signals. IEEE Trans Ultrasound Ferroelec Freq Control 1994;41(6):845–852.

Nelson T, Downey D, Pretorius D, Fenster A. Three-dimensional ultrasound. Lippincott, 1999.

Press WH, et al. Numerical recipes in C. Cambridge, UK: Cambridge University Press, 1994.

Quistgaard J. Signal acquisition and processing in medical diagnostics ultrasound. IEEE Signal Proc Magazine 1997;14(1):67–74.

Rignot E, Chelappa R. Segmentation of polarimetric sunthetic aperture radar data. IEEE Trans Image Proc 1992;1(1):281–300.

Ripley B. Pattern recognition and neural networks. Cambridge, UK: Cambridge University Press, 1996.

Rohling RN, Gee AH, Berman L. A comparation of freehand three-dimensional ultrasound reconstruction techniques. Med Image Anal 1999;4(4):339–359.

Rohling R, Gee A, Berman L, Treece G. Radial basis function interpolation for 3D freehand ultrasound. In: Proceedings of the 16th International Conference on Information Processing in Medical Imaging. Visegrd, Hungary, June 1999. Springer, 1999b:478–483.

Sanches J, Marques JS. A Rayleigh reconstruction/interpolation algorithm for 3D ultrasound. Pattern Recognition Lett 2000;21:917–926.

Sanches J, Marques JS. A Rayleigh reconstruction/interpolation algorithm for 3D ultrasound. Pattern Recognition Lett 2000;21:917–926.

Sanches J, Marques JS. A multiscale algorithm for three-dimensional freehand ultrasound. Ultrasound Med Biol 2002;28:1029–1040.

Sanches J, Marques J. A Fast MAP algorithm for 3D ultrasound. Proceedings Third International Workshop. Energy Minimization Meth Comput Vision Pattern Recog 2001b;63–74.

Sanches J, Marques J. A MAP filter for 3D ultrasound. Proc Int Conf Image Processing 2002.

Shankar P. Speckle reduction in ultrasound B-scans using weighted averaging in spatial compounding. IEEE Trans Ultrason Ferroelec Freq Control 1986;33(6):754–758.

Wells PNT, Halliwell M. Speckle in ultrasonic imaging. Ultrasonics 1981;225.

APPENDIX 1

Fisher–Tippett distribution

Consider the random variable (R.V.) y with a Rayleigh distribution with parameter ψ:

$$p(y) = \frac{y}{\psi} e^{-\frac{y^2}{2\psi}}, \tag{39}$$

and a log-compression law given by: $z = \alpha \log y + \beta$. The distribution of z is given by:

$$p(z) = \left|\frac{dy}{dz}\right| p(y) = \frac{w^2}{\alpha\psi} e^{-\frac{w^2}{2\psi}} \tag{40}$$

where $w = e^{\frac{z-\beta}{\alpha}}$. Rearranging this equation, it becomes

$$p(z) = \frac{2}{\alpha} e^{g - e^g} \tag{41}$$

where $g = e\dfrac{z-\beta}{\alpha} - \log 2\psi$. This is the Fisher–Tippett distribution, often called double-exponential distribution. The mean and variance are obtained through:

$$\bar{z} = \frac{\alpha}{2}(\log(2\psi) - \gamma) + \beta \tag{42}$$

$$\sigma_z^2 = \frac{(\pi\alpha)^2}{24} \tag{43}$$

where γ is the Euler-Masheroni constant ($\gamma = 0.5772$) (Abramowitz and Stegun 1972).

APPENDIX 2

β_0 estimator

In this Appendix, we will show that the estimator

$$\beta_0 = \min(z_i) \tag{44}$$

used for the initialization of the offset parameter β, β_0, used in eqn (8) is biased and its expected value is computed.

Let us consider the set $Y = \{y_i\}$ of observations represented in Fig. 21. It is assumed that the elements y_i are independent and identically distributed with distribution $g(y)$.

Let

$$t = \min(y_i) \tag{45}$$

and the minimum of Y, be a random variable. Let us compute its density probability function $h(t) = p(\min(y_i) = t)$.

Let $P_i(x)$ be the probability of y_i to belong to the interval $[x, x + \Delta]$ and all other elements be greater than $x + \Delta$ (see Fig. 21). This probability is:

$$P_i(x) = \int_x^{x+\Delta} (g(y_i)dy_i) \prod_{j\neq i}^{N-1} \int_{x+\Delta}^{\infty} g(y_j)dy_j \tag{46}$$

Because all the elements of Y are identically distributed

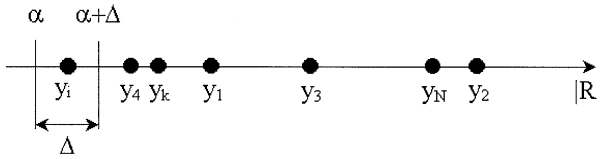

Fig. 21. Graphic representation of a set of random variables.

$$P_i(x) = \int_x^{x+\Delta} (g(y)dy) \left[\int_{x+\Delta}^{\infty} g(y)dy\right]^{N-1} \tag{47}$$

and making $\Delta \to 0$ leads to the density probability function of the minimum of Y

$$p_i(x) = \frac{P_i(x)}{\Delta} = g(x)(1 - G(x))^{N-1} \tag{48}$$

where $G(x) = \int_0^x g(\tau)d\tau$ is the cumulative distribution function of y.

The probability of at least one element of Y being equal to t (*i.e.*, the density probability function of the minimum of Y) is:

$$h(t) = \sum_i p_i(t) = Ng(t)(1 - G(t))^{N-1} \tag{49}$$

Let

$$\beta_0 = \min\{z_i\} \tag{50}$$

with

$$z_i = \alpha \log(y_i + 1) + \beta \tag{51}$$

then

$$\begin{aligned}\beta_0(t) &= \min\{z_i\} = \min\{\alpha \log(y_i + 1) + \beta\} \\ &= \alpha \log(\min\{y_i\} + 1) + \beta = \alpha \log(t + 1) + \beta\end{aligned} \tag{52}$$

leading to the expected value of $\beta_0(t)$

$$E(\beta_0) = \int_0^{\infty} \beta_0(\tau)h(\tau)d\tau. \tag{53}$$

Let us consider the observed data, y_i, as being Rayleigh-distributed with parameter ψ

$$g(y) = \frac{y}{\psi} e^{-\frac{y^2}{2\psi}}. \tag{54}$$

Replacing this expression in eqn (49) leads to:

$$h(t) = N\frac{t}{\psi} e^{-\frac{t^2}{2\psi}} \int_t^{\infty} \left[\frac{\tau}{\psi} e^{-\frac{\tau^2}{2\psi}} d\tau\right]^{N-1} = \frac{t}{\psi'} e^{-\frac{t^2}{2\psi'}}, \tag{55}$$

where

$$\psi' = \psi/N. \tag{56}$$

This result shows that the distribution function of the minimum of a set with N elements with Rayleigh distribution, with parameter ψ, is also Rayleigh–distributed with parameter ψ/N. The larger the number of elements, the closer to zero is the expected value of the minimum.

Let us replace (55) in (53), leading to:

$$E(\beta_0) = \alpha A + \beta \tag{57}$$

where

$$A = \int_0^{+\infty} a(\tau) d\tau, \tag{58}$$

with

$$a(\tau) = \frac{e^{-\frac{\tau^2}{2\psi'}}}{\tau + 1} \tag{59}$$

Because $a(\tau) > 0$ for $\tau > 0$, (58) is greater than zero. Therefore,

$$E[\beta_0] > \beta, \tag{60}$$

(*i.e.*, the estimator $\beta_0 = min(Z)$ is biased and greater than β). The coefficient A depends on ψ', which depends on the amount of data, N; see eqn (46). The larger the amount of data, the smaller is ψ'. In the limit, as the amount of data grows, $\psi' \to 0$, which implies $A \to 0$. Therefore, for a large amount of data, the estimator β_0 can be considered to be unbiased.